

MULTI-TEMPORAL ABRUPT CHANGE ESTIMATION ON LANDSAT TIME SERIES IMAGERY: AN APPLICATION TO ANALYZE BURN SEVERITY IN LA PRIMAVERA, MEXICO

INDER TECUAPETLA-GÓMEZ⁽¹⁾, GABRIELA VILLAMIL-CORTEZ,
AND MARÍA ISABEL CRUZ-LÓPEZ⁽²⁾

ABSTRACT. We analyze 14-years NDVI and dNBR time series of Landsat-7 imagery for monitoring long-term burn severity on an Area of Protection of Flora and Fauna known as La Primavera. We propose a burned area mapping approach that does not require prior knowledge of the fire's date. We begin by applying a statistical algorithm (BFAST) to estimate abrupt changes in the NDVI's trend. The estimated abrupt changes are used as reference dates (plausible fire dates) from which dNBR is calculated following a typical pre-post fire assessment. These dNBR values allow us to determine burned areas and quantify an apparent severity or a sudden regrowth. Unlike most burned area mapping methods ours depends effectively only on one tuning parameter, h ; based on a set of simulations we provide rules to select this parameter. Our simulations also show that when one abrupt change is present in the NDVI's trend, BFAST's performance is appropriate even when 20% of observations are missing in the time series. Also from our simulations, we found that despite that the probability of estimating correctly two abrupt changes deteriorates as the percentage of missing values increases, BFAST's conditional underestimation will cease when the distance between abrupt changes is greater or equal than the sample size times h ; in this case, BFAST does not incur in overestimation. A RapidEye-derived burned area map is used as a reference dataset to validate our procedure; we show empirically that our maps can achieve up to 83% of overall accuracy under moderate data quality (time series in which 47 to 49% of observations are missing). Our approach provides annual burn severity maps that allow us to establish that La Primavera has undergone to a series of statistically significant vegetation changes, plausibly attributed to fire, almost in its entirety throughout the studied period. Despite the latter, we found that most of La Primavera's burned areas have suffered from low severity. R code to implement our approach complements this paper.

1. INTRODUCTION

United Nations conceives the protection, restoration and promotion of a sustainable use of terrestrial ecosystems, sustainable manage forest, combat desertification, and halt and reverse land degradation and halt biodiversity loss as a goal to make the world more sustainable by 2030; cf. UN (2019). In this context, both tools and variables to monitoring

¹CONACyT-CONABIO-DIRECCIÓN DE PERCEPCIÓN REMOTA, LIGA PERIFÉRICO-INSURGENTES SUR 4903, PARQUES DEL PEDREGAL, TLALPAN 14010, CIUDAD DE MÉXICO

²COMISIÓN NACIONAL PARA EL CONOCIMIENTO Y USO DE LA BIODIVERSIDAD (CONABIO)
E-mail addresses: itecuapetla@conabio.gob.mx, gaby22_cortez@hotmail.com, icruz@conabio.gob.mx.

Date: May 17, 2022.

Key words and phrases. breakpoint estimation, BFAST, NDVI, dNBR, time series, burn severity maps, missing values, La Primavera, Landsat-7, mapping burn areas.

This research was partially supported by CONACyT grant APN2016-2760.

vegetation characteristics under human induced pressure are essential. One of these variables is *fire*, a natural element, that as a climate variable contributes to characterize Earth's climate conditions GCOS (2019). It might not be obvious but fire provides benefits to some ecosystems but inflicts major losses on others, see, e.g. Whelan (1995) and Pyne (1997).

An effective means to contribute to the protection of terrestrial ecosystems, in particular forest, as well as halting land degradation and biodiversity loss is through the correct assessment of wildfires. For example, at a global scale, wildfires may contribute to alter the greenhouse gas emissions' equilibrium and at a local scale may be a factor in biodiversity loss and land degradation, cf. Chuvieco (2009). An indirect approach to assess wildfires consists of using some of the several satellite-derived products (which are available at different scales) and apply a sounding method for mapping burned areas and quantify their severity levels (when severity exists).

For instance, Ch. 10 of Chuvieco (2009) presents an encyclopedic treatment of the many efforts to combine different sensors, satellite-derived products, identification techniques, assessment and monitoring of burned areas, see also Chuvieco et al. (2019) for recent developments in this research field.

In order to identify burned areas we have to consider three basic aspects 1) fuel presence (in this case, vegetation) 2) abrupt changes in certain spectral indices and 3) persistence of the abrupt change over time, cf. Chuvieco et al. (2008). Following these principles, several strategies and spectral indices have been used for mapping burned area. Some researchers have considered monitoring changes in the structure of the Normalized Differenced Vegetation Index (NDVI) as an effective tool for determining burned areas, cf. Chuvieco and Congalton (1988), Caetano et al. (1996), Rogan and Yool (2001), Díaz-Delgado (2003) and Cocke et al. (2005), among many others.

Key (2006) sets a conceptual ground contributing to a better understanding of burn severity. Basically, among the efforts for determining burn severity we can distinguish those that consider an initial assessment of the impact of fire (short-term) and those which are advocated to an extended assessment of the impact of fire (long-term), see also Van Wagtendonk et al. (2004) for similar considerations. For a handful of investigations that have focused on the long-term aspect of burn severity analysis, we refer to Miller and Yool (2002), Van Wagtendonk and Root (2003), Eidenshink et al. (2007), Giglio et al. (2009), Boschetti et al. (2015), Roy et al. (2019) and Campagnolo et al. (2019). In this work we propose a method that contributes to the long-term analysis of burn severity by studying abrupt changes in the NDVI's trend structure and changes in the magnitude of the difference Normalized Burn Ratio (dNBR). The quantitative and physical characteristics of NBR and dNBR as variables to assess burn severity have been evaluated amply, cf. Miller and Yool (2002), Van Wagtendonk et al. (2004), Epting and Verbyla (2005), Brewer et al. (2005), Chuvieco et al. (2006), Key and Benson (2006), Roy et al. (2006), Miller and Thode (2007).

As in this work, other authors have used Landsat time series of spectral indices for mapping burned area. For instance, Stroppiana et al. (2011) apply fuzzy set theory methods to multiple spectral indices and propose a region growing algorithm to determine burn areas. Goodwin and Collett (2014) used the sum of bands 4 and 5 as a burned area index to which applied temporal smoothing (via moving medians of order 7 and seasonal medians) to remove potential outliers, the resulting *smoothed* time series are taken as *no change* references, finally, proposed to call potential core burned area pixels to those pixels at which

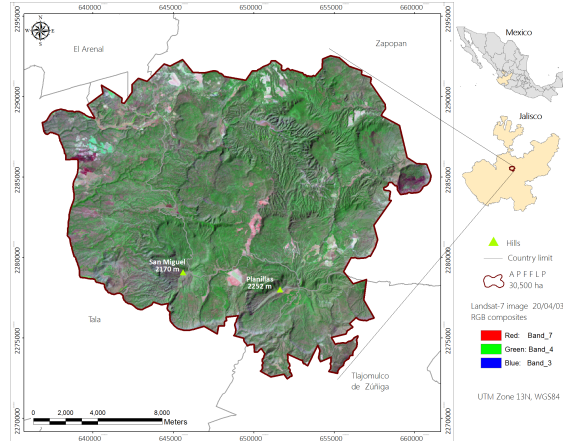


FIGURE 1. Geographic location of Flora and Fauna Protected Area *La Primavera*.

the difference of the original time series and the reference exceeds certain threshold; thresholding is based on experimentation and expert opinion. Hawbaker et al. (2017) proposed an algorithm that uses radient boosted regression models to generate burn probability surfaces based on a series of variables and tuning parameters such as band values and spectral indices from individual Landsat scenes, lagged reference conditions, and change metrics between the scene and reference predictors. Burn classification is generated from the burn probability surfaces using pixel-level thresholding in combination with a region growing process. The algorithm can be applied anywhere Landsat and training data are available. These papers employed most of the Landsat collection, see also Zhao et al. (2015), generating time series longer than the one used in the present work as we only considered Landsat-7 images. Contrary to Hawbaker et al. (2017), which use a probabilistic criterion to call for a burned pixel, Goodwin and Collett (2014) do not base burn mapping on statistical or probabilistic principles, hence it is not possible to quantify the significance or likelihood of an estimated burned pixel.

Unlike most of the aforementioned methods for mapping burned area, ours does not require prior knowledge of the fire’s date. Indeed, we begin by determining *statistically* abrupt changes in the NDVI’s trend structure; to this end we apply Verbesselt et al. (2010a)’s BFAST. Since these changes may have different origins, for instance deforestation, we utilize auxiliary information to properly link them with burn events. We use the estimated abrupt change as the reference (date of fire) to perform a typical pre-post fire assessment. In order to do so, we calculate the dNBR as it assesses accurately the magnitude of change in the vegetation condition due to fire, cf. Robichaud et al. (2007). Having calculated the dNBR value, we also quantify burn severity in a temporal vecinity of the estimated date of fire, see Section 3.3 for further details. The combination of NDVI and dNBR to assess burn severity has also been considered by Escuin et al. (2008) in areas which are similar to La Primavera, our area of study. La Primavera is an Area of Protection of Flora and Fauna contained by the path-row 29-40 of Landsat-7 images, see Fig. 1 above; in this paper we utilize every available image (an suitably pre-processed) from 2003 to 2016, see Section 2.

Another distinctive feature of our method is that, effectively, we only need to tune in a single parameter in BFAST. This parameter, $0 < h < 1$, controls a smoothing process associated with the test statistic to determine abrupt changes. The existing rules for choosing

h are applicable when the time series are complete, cf. Section 2.2 of Verbesselt et al. (2010b). Because some images of our datasets showed a large amount of missing data ($\sim 60\%$ of pixels), once images datacubes are assembled, we applied temporal interpolation (linear and spline-based) to fill the gaps. Via simulations we assessed the influence of these two interpolation methods, the amount of missing values, and the value of h on the statistical estimation of the breakpoints of our NDVI time series (Section 4).

From our simulations we found that regardless of h and the percentage of missing values, the probability coverage of identifying one abrupt change is greater when using the spline interpolation method than when using the linear one. In the same case, we also found that the correct estimation probability is greater, at least marginally, when using linear interpolation than when using spline and when the missing data ranges from 40 to 60%. Using MSE as a measure of accuracy, we found that up to 20% of missing values, BFAST’s performance is appropriate independently of the parameter h and interpolation method. From 30% and upwards, the combination of linear interpolation and BFAST outperforms the combination of spline interpolation and BFAST. We also studied the performance of BFAST in estimating two breakpoints under the scenario of missing values. Although the probability of correct estimation in this case deteriorates as the percentage of missing values increases, we found that BFAST’s underestimation will cease when the breakpoints are separated by an amount of time-points larger or equal to the sample size times h and we did not find overestimation. In light of this, in our application we used linear interpolation to fill missing values and $h = 0.15, 0.23$ as BFAST’s tuning parameter.

A RapidEye burned area map is used as a reference dataset to validate our procedure; we show that our maps can achieve up to 83% of overall accuracy as data quality is optimal, see Section 5.2. Despite the apparent high density of missing values in our datasets we show that burned areas are properly identified given rise to a series of reliable annual burn severity maps. These maps allow us to establish that La Primavera has undergone to a series of statistically significant vegetation changes almost in its entirety throughout the studied period. Although constantly affected by fire, we found that most of La Primavera’s burned areas have suffered from low severity. We use the statistical software R to conduct all our analysis and a copy of our code is available at the GitHub repository <https://github.com/inder-tg/burnSeverity>.

2. AREA OF STUDY AND DATA SETS

2.1. Area of study. We are concerned with the Area of Protection of Flora and Fauna La Primavera (APFFLP) which has an area of 30.5 ha and is located in the central region of the Jalisco state, between the Universal Transverse Mercator (UTM) coordinates 635 040 E; 2 295 019 N and 661 815 E; 2 273 893 N zone 13 North (Figure 1).

The APFFLP lies on sierra La Primavera, which geographically is to the west of Guadalajara City (capital of Jalisco), the third more important city in Mexico, physiographically belongs to the province of Eje Neovolcánico. Due to its volcanic origin La Primavera is one of the most diverse volcanic reliefs in Mexico, where annular domes, plateaus, hills and mountains follow the fracture lines of the volcanic caldera and irregular hills modeled by erosion; these formations are also influenced by fluvial and tectonic forces.

The highest peak of La Primavera is Cerro Planillas followed by Cerro San Miguel which are both located in the southern part of the protected area. Towards the west, the relief is constituted by hills. The valleys located around are plains originated by depositions of foams contributed by La Primavera formation; the physiographic variation is between 1380 and 2250 m, see Semarnat (2000).

According to INEGI (2016)'s classification there are four types of vegetation: oak forest (*Quercus*), oak-pine forest (*Quercus-Pinus*), pine-oak forest (*Pinus-Quercus*) as well as secondary shrub vegetation that develops within the different types of vegetation just mentioned. There is also induced grassland and agriculture. The most representative vegetation is the oak-pine forest.

Despite being an area of protection, La Primavera's different types of forests are in constant fire danger. In the 2003-2016 period the largest fire was recorded in April 2005 (8.4 ha) followed by another in April 2012 (8.3 ha), cf. del Castillo (2006) and Delgado-Morales (2012). Huerta-Martínez and Ibarra-Montoya (2014) report on fires from 1998 to 2012 and state agencies have recorded fires in 2010, 2013 and 2016. This high frequency of fires may be due to a combination of many activities developed in La Primavera such as agricultural burns, the accumulation of organic matter, fire pits, cigarette residues and burning in clandestine landfills.

2.2. Data sets. We utilize Landsat-7 images from the path-row 29-40; these scenes were downloaded from the U.S. Geological Survey repository (<https://earthexplorer.usgs.gov/>). In order to calculate the NDVI and NBR we only need spectral bands 4, 5 and 7 (with 30 m spatial resolution). These bands were processed at the L1T level of surface reflectance (via LEDAPS by Vermote et al. (1997)) with a proper cloud masking (via FMASK by Masek et al. (2006)). We projected these images to the UTM and ellipsoid WGS84 system.

In this study we consider scenes from January 2003 to December 2016. Among the 322 expected scenes only 238 were actually available. Additionally, we have to factor in 22% (roughly) of missing data due to the failure of the Landsat Scan Line Corrector, cf. Zhang et al. (2007). Later, we will explain how we dealt with these important amount of missing data. Besides this unfortunate lack of information Landsat-7 images are still an important asset in the Landsat repository, particularly once Landsat-5 was discontinued, cf. Landsat Missions (2016).

2.2.1. Reference data.

Over the last 2 decades some fire affected zones in La Primavera have been recorded by some governmental agencies. When possible this data is recorded in situ. In most cases, however, fire assessment has been performed through methods that utilize satellite images. This information is typically distributed in a raster or polygon format. Figure 2 shows polygons of estimated burned areas based on MODIS and RapidEye images.

For 2012, we produce a RapidEye polygon used, see Section 5.2, to assess the overall accuracy of a burned area map obtained by our methodology. In order to obtain this polygon we utilize NDVI and an index of burned area proposed by Martín and Chuvieco (2001) both derived from 4 RapidEye images with spatial resolution of 5 m; a standard radiometric correction was applied to get TOA reflectance. In this RapidEye polygon the estimated burned area depends on empirical thresholds which were chosen based on visual inspection.

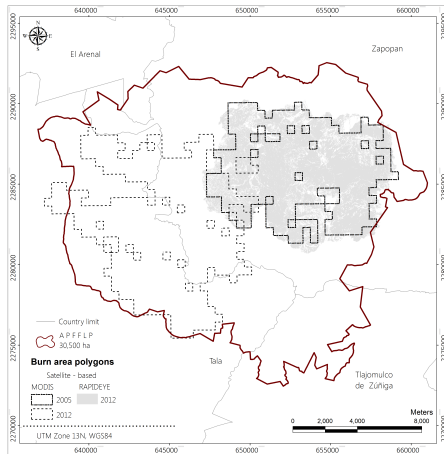


FIGURE 2. Polygons of estimated burned areas based on MODIS and RapidEye images in La Primavera.

3. METHODOLOGY

Our approach is comprised by 4 stages. Firstly, we generate time series of Landsat-7 satellite images. Secondly, we apply the breakpoint estimation method known as BFAST to the NDVI data cube. Thirdly, utilizing the estimated breakpoint (date) as reference we calculate its dNBR using to this end two NBR values, one before and another after the estimated breakpoint; this dNBR value will indicate whether a breakpoint can be linked to a fire event. Finally, based on the dNBR, and following Key and Benson (2006), we propose to classify the breakpoint as a fire event (with some level of severity) or as a (low or moderate) vegetation regrowth. Now we will explain each of these stages in more detail.

3.1. Time series generation. First of all we created a *stack* with our collection of Landsat images. In those instances in which the scene was missing we created an image full with NA (not available); NA is the R symbol for missing data. We do not consider the entire extent of a Landsat scene but only a rectangle large enough to cover La Primavera. After this arrangement we end up with a data cube with 900×1000 columns \times 322 scenes entries.

As said previously we applied a mask, derived from the FMASK algorithm, to those images containing clouds and cloud shadow. This procedure is rather standard and has been used by White et al. (2014), Hermosilla et al. (2015) and Foga et al. (2017) among many others. For consistency with our R-based code we replaced the fill value of this cloud mask by an NA.

In order to fill in the NA values in our data cubes (NDVI and NBR) we applied linear and spline-based interpolation at the temporal level, that is, we did not utilize any spatio-temporal approach. More precisely, we employed the methods `linear` and `spline` from the R package `imputeTS` by Moritz and Bartz-Beielstein (2017). In Section 4, we assess the influence of these interpolation methods on the statistical estimation of abrupt changes of simulated NDVI time series.

3.2. Abrupt change detection with statistical guarantees. In order to estimate statistically abrupt changes in the trend structure of our NDVI time series we applied BFAST, a method implemented in an R package with the same name, cf. Verbesselt et al. (2012). Briefly speaking, BFAST tests whether there are abrupt changes (both in the trend and

seasonal components) in a time series and when this statistical test is *significant* (at a level set by the user) then the time series is divided in as many segments as (significant) detected abrupt changes. In this paper we utilize the default significant level ($\alpha = 0.05$) but we stress that the user is allowed to decrease α and get less abrupt changes (the conservative viewpoint) or increase it and potentially obtain more changes (from a more risk-oriented viewpoint).

To be a bit more precise, let us assume that y_t denotes the value of an NDVI time series at time t . BFAST begins by assuming the following additive representation for y_t :

$$y_t = T_t + S_t + \varepsilon_t, \quad t = 1, \dots, n, \quad (1)$$

where T_t represents the piecewise linear function

$$T_t = \alpha_j + \beta_j t, \quad \tau_{j-1} \leq t \leq \tau_j$$

with breakpoints at $0 = \tau_0 \leq \tau_1 \leq \dots \leq \tau_m$, S_t describes a seasonal component, ε_t denotes white noise with constant variance σ^2 , and n is the sample size.

A priori m (the total number of breakpoints), the location of the breakpoints (τ_j s) and both the intercept (α_j) and the slope (β_j) of each linear segment are unknown. The purpose of BFAST is to estimate all of these parameters in a reasonable time and with statistical guarantees. The estimation of m , known as model selection, is done by virtue of minimizing the so-called Bayesian Information Criterion (BIC). Estimates for the breakpoints τ_j s are the result of an ordinary least squares problem whereas estimates for α_j and β_j are the solution of a so-called M -estimation problem. The computational strategy that makes possible that these multiple estimation procedures are done *fast* is known as *dynamic programming*. The statistical test used to determine the existence of multiple abrupt changes is known as OLS-MOSUM; we will elaborate a bit more about this test in Section 4 as it will play a role in our simulation setups.

As of today BFAST has been used in multiple applications to assess different types of changes in the vegetation of several ecosystems, e.g. Watts and Laffan (2014), DeVries et al. (2015), Dutrieux et al. (2015), Schultz et al. (2016), Zewdie et al. (2017) and Wu et al. (2018).

We did not discuss the seasonal component representation above as we are focused on estimating abrupt changes in the trend component only. For details about the seasonal component, or the BFAST implementation in general, we refer to the original papers of Verbesselt et al. (2010a,b).

3.3. How to calculate a burn severity map? Let $\hat{\tau}_k$ denote the k -th estimated breakpoint in an NDVI time series given by BFAST. Since the sheer presence of an abrupt change in the NDVI structure is not sufficient to determine a burn event, we consider that there has to be also a change in the value of the NBR in a neighborhood of the breakpoint $\hat{\tau}_k$.

Since we use Landsat-7 images and the dominant vegetation of La Primavera is the forest of oak-pine we follow Escuin et al. (2008) who have shown that the dNBR is an appropriate variable to assess wildfire severity in forest vegetation. More precisely, given $\hat{\tau}_k$, its corresponding dNBR is defined as

$$\text{dNBR}(\hat{\tau}_k) = \text{NBR}_{\hat{\tau}_k-23} - \text{NBR}_{\hat{\tau}_k+1}.$$

Note that the time-point $\hat{\tau}_k - 23$ corresponds to almost a year earlier than the estimated breakpoint $\hat{\tau}_k$ whereas $\hat{\tau}_k + 1$ is the time-point right after the estimated vegetation change.

dNBR	Regrowth	Severity
< -0.25	High	
-0.25 to -0.1	Low	
-0.1 to 0.1		Unburned
0.1 to 0.27		Low
0.27 to 0.66		Moderate
> 0.66		High

TABLE 1. Types and levels of vegetation’s changes.

As argued by Escuin et al. (2008) considering these two dates, and their corresponding NBR values, minimizes the differences specifically linked to phenological changes or illumination conditions.

Having calculated $dNBR(\hat{\tau}_k)$ now we employ the values of Table 1, adapted from Key and Benson (2006) (see also Lutes et al. (2006)), to classify the type of vegetation affectation near $\hat{\tau}_k$; in Key and Benson (2006)’s table the category of regrowth is considered as a type of severity and there is a distinction between low and high moderate severity. Based on this table we are able to characterize areas under vegetation regrowth and areas that have suffered some kind of burn severity.

It has been documented, see Section 4.2 of Verbesselt et al. (2010a), that summarizing the breakpoint estimated by BFAST to a year level ease comparison. We followed this approach to produce our NDVI change and burn severity maps. These maps will be presented in Section 5. In the following section we assess the performance of BFAST for estimating breakpoints under the absence of observations in the time series.

4. PARAMETER CALIBRATION UNDER MISSING VALUES

Since our collection of Landsat images has a high density of missing values, it becomes relevant to understand BFAST’s performance in this scenario. In this section we assess the performance of BFAST in estimating one and two abrupt changes once linear or spline-based interpolation has been applied to fill some simulated missing values. To this end, we will simulate NDVI time series sharing the main features exhibit by the *real* Landsat-7 NDVI time series used in our application.

4.1. Parameters for simulations setup. We simulate 16-day NDVI time series from 2003 to 2016 obeying the additive representation given by Eq. (1). The seasonality (S_t) and the white noise (ε_t) of these synthetic time series are described with a harmonic regression model and random samples of a normal distribution with zero mean and standard deviation (s.d.) σ , respectively. For the amplitude parameter needed to fit the harmonic model we consider 0.15 and 0.3; for simplicity we use a 0° phase angle. We consider $\sigma = (0.02, 0.05, 0.07)$ as these values are in line with the variability level of our analyzed NDVI time series.

Our data cubes suffer from an important lack of observations. For instance, nearly half of the NDVI time series in the studied area lacks of at least 54% of observations, see Figure 11-A in the next section. We *simulate* missing values as follows. From the 322 time-points of any simulated time series (y_t) we choose randomly and without replacement, t_1, \dots, t_P say, points. Then the corresponding value in the time series is masked as *not available*, that is, we set $y_{t_i} = \text{NA}$, where $i = 1, \dots, P$. In the simulations below we use $P = 0, 32, 64, 97, 129, 161, 194$, values which correspond to roughly 0, 10, \dots , 50 and 60% of the total observations.

h	methods	% of missing values						
		0	10	20	30	40	50	60
0.15	Linear	99.2	97.9	92.7	79.0	55.9	29.1	10.9
	Spline	99.2	98.2	92.4	83.1	68.9	55.6	41.5
0.23	Linear	99.9	99.7	97.6	92.1	80.5	60.3	39.9
	Spline	99.9	99.3	97.4	93.6	88.3	79.8	68.6
0.45	Linear	100	100	100	100	100	100	100
	Spline	100	100	100	100	100	100	100

TABLE 2. Probability coverage of estimating one breakpoint as a function of the bandwidth h . Here $\sigma = 0.02$ and amplitude 0.15.

As mentioned above BFAST utilizes the OLS-MOSUM test to determine statistically the existence of abrupt changes. As explained, for instance in Chu et al. (1995) and Zeileis et al. (2002), this test is based on a sequence of partial sums of ordinary least-squares residuals; the number of residuals in each sum is fixed, approximately nh , but controlled by a *bandwidth* parameter $0 < h < 1$. Although there are some empirical rules for the value of h , cf. Section 2.2 of Verbesselt et al. (2010b), our data set does not quite meet the conditions for these rules to be applied, specially due to the large amount of missing data. Hence, we also include h as a parameter in our simulations; we select $h = 0.15, 0.23, 0.45$.

Each simulation study was repeated 1000 times and we use metrics such as probability coverage and mean squared error (MSE) to assess them. In the next subsections we will specify the trend structure, T_t , as this is different in each study.

4.2. Assessing BFAST’s performance in estimating one breakpoint. In this study the trend has a single breakpoint at the observation 161. Before this breakpoint the trend is constant (0.7) and after follows the line $0.3 + 0.2/161 t$. More precisely and following Eq. (1), $n = 322$, $\alpha_1 = 0.7$, $\alpha_2 = 0.3$, $\beta_1 = 0$, $\beta_2 = 0.2/(161)$, $\tau_0 = 0$, $\tau_1 = 161$, $\tau_2 = 322$ and $m = 2$.

As a first goal we are interested in the *probability coverage* of BFAST for estimating one breakpoint, i.e., the number of times in which a breakpoint is detected divided by the number of simulations, as a function of the s.d. of the errors of model (1), interpolation method, percentage of missing values, amplitude of the seasonal component and the bandwidth value h utilized by BFAST.

Since a small s.d. benefits both interpolation methods, see Table 7 and its discussion in the Supplementary Materials, here we present the results of simulations when we set $\sigma = 0.02$ (the smaller value of σ under consideration) and allow the bandwidth parameter to vary.

We begin by discussing the results of Table 2. BFAST’s probability coverage increases with the bandwidth regardless of the interpolation method. The probability coverage is remarkably large when $h = 0.45$. For a time series of 322 observations, $h = 0.45$ is equivalent to using a bandwidth of 145 time-points in the aforementioned OLS-MOSUM statistic; this amount of time-points is roughly 6 years in the Landsat temporal scale. From our next simulation study (Section 4.3) we infer that utilizing $h = 0.45$ in our real data application is equivalent to requiring that the separation between two breakpoints be of roughly 6 years. Due to this and because our a priori information reports vegetation changes in 2005, 2010, 2012 and 2013, we will not use $h = 0.45$ in our application. For $h = 0.15, 0.23$ the probability coverage decreases as the percentage of missing values increases. Regardless of h and the missing values percentage, the probability coverage is greater when using the spline interpolation method than when using the linear one. Similar results are found when the

h	methods	% of missing values						
		0	10	20	30	40	50	60
0.15	Linear	100	91.7	80.5	69.7	58.9	53.6	42.2
	Spline	100	91.4	80.2	70.2	60.8	47.8	37.1
0.23	Linear	100	91.4	80.6	70.6	60.2	53.4	45.1
	Spline	100	91.2	80.1	69.9	60.9	49.6	36.3
0.45	Linear	100	91.4	80.5	70.2	60.3	52.6	42.4
	Spline	100	91.3	80.1	70.0	61.7	50.0	37.0

TABLE 3. Correct estimation probability coverage for one breakpoint when h varies. Here $\sigma = 0.02$ and amplitude 0.15.

amplitude increases with the additional feature that the probability coverage is marginally greater than in the present case, see Tables 8 and 9 in the Supplementary Materials.

We also assess BFAST’s *correct estimation* probability coverage, that is, conditioned on having estimated a breakpoint, we computed the number of times in which the BFAST estimate coincides with the true breakpoint, $\tau_1 = 161$, when h varies but $\sigma = 0.02$, see Table 3. According to this table BFAST has an outstanding correct estimation probability coverage for one breakpoint when the time series *does not* have missing values. As the amount of missing values in a time series increases then the correct estimation deteriorates. Moreover, from this table we can infer the following result. Let $0 < p < 1$ be given. When $100 \times p\%$ of observations are missing in a time series and BFAST has estimated one breakpoint, then the probability that this is the true breakpoint is close to $1 - p$. Additionally, this table suggests that the correct estimation probability is greater, at least marginally, when using linear interpolation than when using spline and when the missing data ranges from 40 to 60%. This is relevant for our application as we deal with a fair amount of time series whose lack of observations ranges in that interval. The same conclusions about the correct estimation probability can be drawn when the size of the amplitude in the seasonal component increases, see Tables 10 and 11 in the Supplementary Materials.

Finally, the accuracy and precision of BFAST in estimating a breakpoint correctly is reported via the MSE. Figure 3 shows that up to 20% of missing values, BFAST’s performance is appropriate independently of the parameter h and interpolation method. From 30% and upwards, the combination of linear interpolation and BFAST outperforms the combination of spline interpolation and BFAST.

4.3. Assessing BFAST’s performance in estimating two breakpoints.

Here we are interesting in assessing BFAST’s ability in estimating two breakpoints as a function of the distance between them and when we set $\sigma = 0.02$, $h = 0.15, 0.23$, vary the percentage of missing data (from 40 to 60%) and utilize a harmonic regression model to simulate the seasonal component (amplitude 0.15 and phase angle 0). We focus on the behavior of BFAST when 40 to 60% of observations are missing in a time series based on the results of our previous simulation and because this amount of missing information is relevant for our applications.

In this study the trend function is defined through Eq. (1) with $\alpha_1 = 0.7$, $\alpha_2 = 0.3$, $\alpha_3 = \alpha_2$, $\beta_1 = 0$, $\beta_2 = 0.2/161$, $\beta_3 = \beta_2$, $\tau_0 = 0$, $\tau_1 = 100$, $\tau_2 = \tau_1 + \ell$, and $\tau_3 = 322$. Observe that the second breakpoint, τ_2 , is separated from the first one (τ_1) by ℓ time-points and we will use $\ell = 10, 20, \dots, 130, 140$.

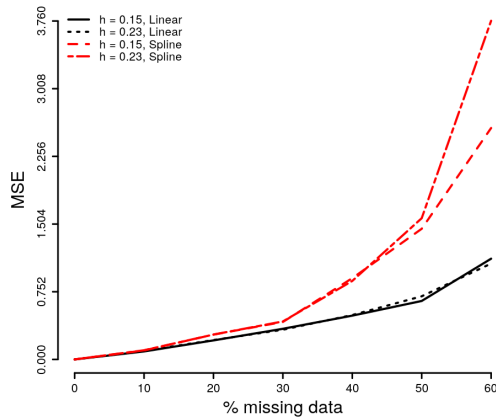


FIGURE 3. MSE of BFAST for estimating a breakpoint with the parameters introduced in Table 2.

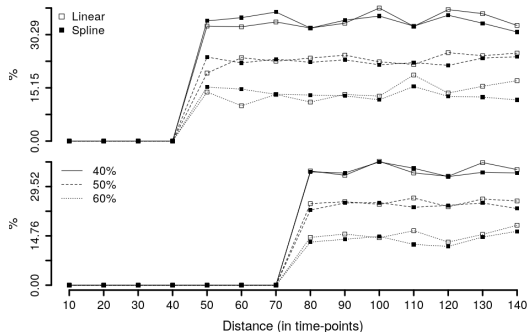


FIGURE 4. Probability coverage. Bandwidth: $h = 0.15$ (top row), $h = 0.23$ (bottom row).

We begin by studying BFAST’s probability coverage of estimating *correctly* the 2 true breakpoints. That is, we divide the number of times in which BFAST estimates the true breakpoints τ_1 and τ_2 by the number of times in which 2 breakpoints are estimated. According to Figure 4, the less percentage of missing data (40%) the greater the BFAST’s probability coverage, regardless of the interpolation method. Also from that figure (top row, $h = 0.15$) we infer that for a correct estimation of two breakpoints these have to be separated by at least 50 time-points (approx. 2 years in Landsat time scale); this is in line with the fact that when $h = 0.15$ the OLS-MOSUM statistic uses a bandwidth with roughly 48 time-points. Similarly, (bottom row) when $h = 0.23$ (and roughly 75 time-points are used in OLS-MOSUM’s bandwidth) BFAST begins to detect two breakpoints as soon as they are separated by at least 80 time-points.

Next, we report on BFAST’s underestimation, see Figure 5 for case $h = 0.23$. We consider underestimation, i.e. either τ_1 or τ_2 are estimated correctly, when one (top row), two (middle row) or more than two (bottom row) breakpoints are detected. In the first case, and regardless of the interpolation method, when 40% of data are missing BFAST only underestimates when the separation between τ_1 and τ_2 is lesser than 60 time-points. In the second case (when two breakpoints are detected), independently of the percentage of missing

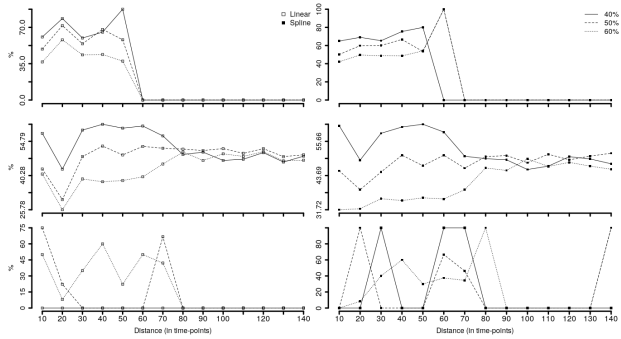


FIGURE 5. Underestimation. Bandwidth $h = 0.23$. Interpolation methods: left column (linear), right column (spline).

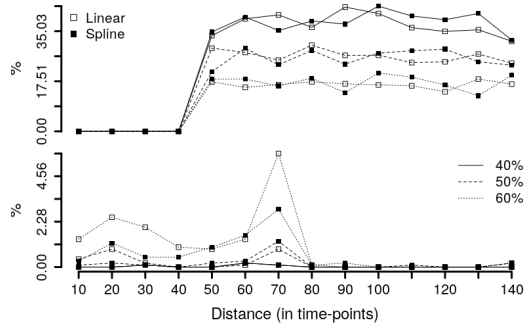


FIGURE 6. Overestimation. Bandwidth: top row ($h = 0.15$), bottom row ($h = 0.23$).

data and the interpolation method, BFAST’s underestimation reaches a stable level (45%) once the separation is about 80 time-points. Finally, once BFAST has detected more than two breakpoints the first thing to notice is that the linear interpolation method shows a less erratic behavior of the underestimation phenomenon throughout different levels of missing data. Also, BFAST’s underestimation will cease when the breakpoints are separated by 80 time-points.

In the Supplementary Materials, see Figure 13, we discuss BFAST’s underestimation for $h = 0.15$. Briefly, in this case, independently of the separation of τ_1 and τ_2 , BFAST will estimate more than two breakpoints and when this occurs only in half of the times one true breakpoint is estimated correctly.

We finalized by reporting that when the distance between two breakpoints is at least 80 time-points and the bandwidth parameter has been set to $h = 0.23$, BFAST does not exhibit an apparent overestimation; this feature is independent of the interpolation method and percentage of missing values, see bottom row of Figure 6.

In light of the results of this section, in the following we will apply BFAST to time series which have been linearly interpolated. Also, since using only $h = 0.23$ precludes the detection of burned areas in 2005, we will utilize the value $h = 0.15$ too and comment on the characteristics of the burned severity maps resulting from the use of each of these values.

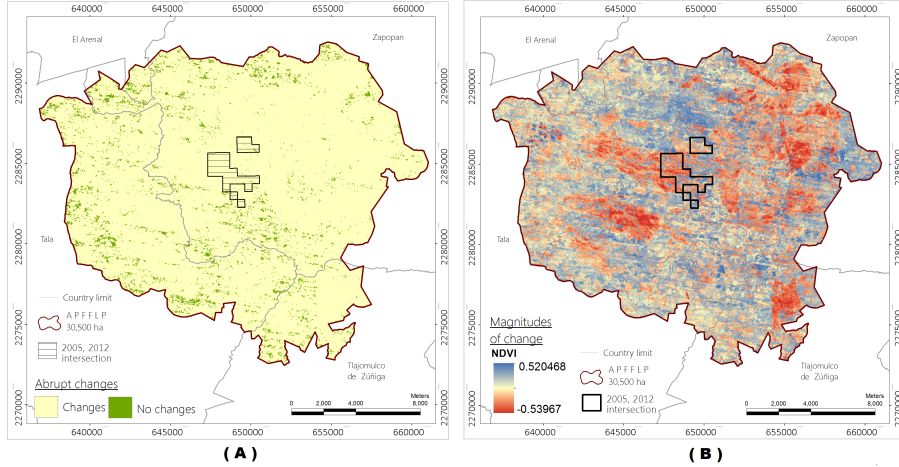


FIGURE 7. Magnitude and change maps. (A) BFAST detected changes 2003-2016. (B) BFAST estimated magnitude of changes 2003-2016.

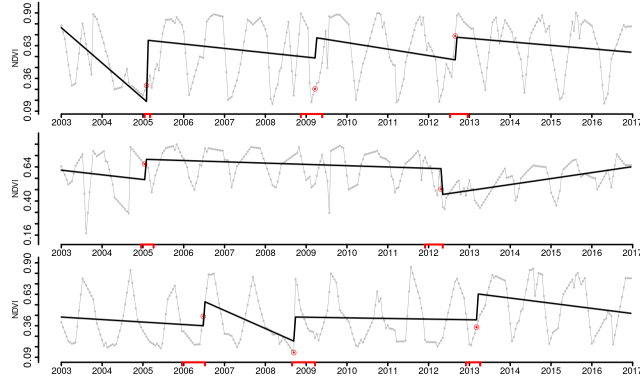


FIGURE 8. BFAST applied on some NDVI pixels. Real data (gray points), estimated breakpoint (red point surrounded by circle), estimated trend (solid line), 95% confidence interval (red).

5. RESULTS AND DISCUSSION

Based on Eq. (1) we can calculate the *magnitude* of the change (perturbation) of an NDVI time series. Verbesselt et al. (2010a), define the magnitude of an abrupt change at the breakpoint τ_j as

$$\text{Magnitude}(t) = \alpha_{j-1} - \alpha_j + (\beta_{j-1} - \beta_j) t.$$

Observe that this is the difference between $T_{\tau_{j-1}}$ and T_{τ_j} , see Eq. (1). Thus, when BFAST detects an abrupt change (significant at 95%), reporting on the magnitude of the largest abrupt change contributes to identify increasing and decreasing regimes in the biophysical variable (vegetation greenness). According to Figure 7, the overall trends of La Primavera's NDVI time series has undergone to a series of (statistically significant) changes almost in its entirety and throughout the studied period, see Figure 7.

Combining the map of reference data and that of change's magnitude, Figure 2 and Figure 7-B, respectively, we can observe those changes which are arguably associated with fire

events. For instance, in Figure 7-**B** we highlight the intersection between the 2005 and 2012 burned areas, from this zone we extract some pixels which are shown in the top and middle row of Figure 8. Based on these figures, at the abrupt change reported in 2005, the estimated trend reports a visible modification, its slope went from negative to positive quite rapidly. Although before 2005 the estimated trend is slightly decreasing we can observe an increase of the NDVI practically right after the estimated breakpoint. Moreover, the annual NDVI cycles are, in average, around 0.6 and this feature is persistent until 2012. It is plausible that this fire has allowed a vegetation re-growth in that area. Unlike the fire reported in 2005, according to the estimates, in 2012 (middle row of Figure 8) the vegetation might have been more drastically affected. In this case, around the breakpoint, the estimated trend has a smaller slope than that of 2005. Also, the NDVI cycles show small amplitudes and only up to the final observation of 2016 the NDVI value went back (approximately) to what it was before the abrupt change of 2012.

The pixel shown in the bottom row of Figure 8 corresponds to an area in which a fire was reported in 2008 and describes decreasing trend regimes. These changes can be construed as marginal compared with the overall structure of the annual NDVI cycles. In 2008, however, the NDVI value achieved its minima over the 14 years under consideration which is in line with the type of affectation caused by a fire. Interestingly, a record about the 2008 fire is only available locally, cf. Huerta-Martínez and Ibarra-Montoya (2014).

These examples illustrate how BFAST can be employed to detect and characterize changes associated with the vegetation’s health. This method also allows us to monitor re-growth regimes when they exist. The difficulty of pursuing this analysis at the pixel level led us to propose a series of maps to visualize vegetation changes and then link these changes with fire events. Some of these maps are presented and discussed now.

5.1. Burn severity maps for La Primavera. According to Key and Benson (2006) we can measure the damage or perturbation inflicted by fire on an ecosystem by reporting its burn severity. Our approach to quantify burn severity is based on BFAST’s breakpoint estimate of the NDVI and then computing the value of the difference in NBR in a vicinity of the breakpoint, see Section 3.3.

Figure 9 summarizes the burned areas detected by our approach and their corresponding severity level. We report the total burned hectares (Table 4) and, relative to this total, the burned area’s fraction classified by severity level (Table 5). There are differences in the estimated total hectares when using either $h = 0.15$ or $h = 0.23$. These differences are specially marked at the extremes of the period (2006 and 2013).

Table 5 shows that the detected burned areas are mainly grouped on the low severity level across 2005-2014. Because high burn severity has been identified as a cause for high erosion rates as well as low vegetation recovery, cf. Doerr et al. (2006) and Moody et al. (2013), we can infer that most of La Primavera’s burned areas suffer from low erosion and profit from a high vegetation regrowth rate.

Our approach detects the two major fires occurred in La Primavera in the 2003-2016 period. Figure 10-**A** reports on the 2005 burned area (using $h = 0.15$) from which the majority has been classified by low followed by moderate and, to a far less degree, high severity. The vegetation affected in this area was primarily native and induced grasslands followed by shrubs and bushes and to a lesser extent adult woodland (oak-pine forest).

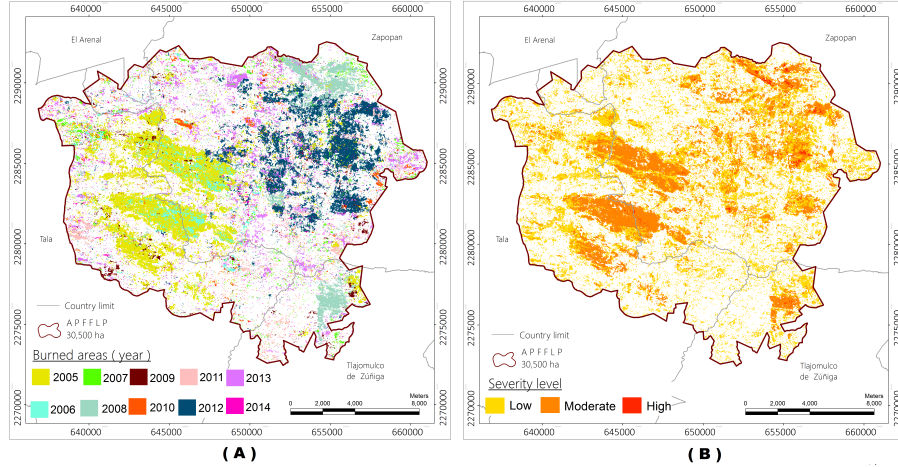


FIGURE 9. Burn severity maps. (A) Estimated burned areas 2003-2016. (B) Severity level of areas shown in (A).

Year	Total burned area (ha)	
	0.15	0.23
2005	3549.24	NA
2006	189.27	729.33
2007	437.58	482.01
2008	1793.34	1156.78
2009	499.86	304.45
2010	402.84	327.18
2011	645.48	620.86
2012	2594.97	2180.61
2013	839.16	1596.44
2014	454.95	NA

TABLE 4. Estimated burned hectares in La Primavera by year. Here NA stands for *not available*.

Year	Severity Level					
	Low		Moderate		High	
	$h = 0.15$	$h = 0.23$	$h = 0.15$	$h = 0.23$	$h = 0.15$	$h = 0.23$
2005	0.648	NA	0.349	NA	0.003	NA
2006	0.888	0.775	0.108	0.224	0.004	0.001
2007	0.922	0.933	0.077	0.067	0.001	0.000
2008	0.695	0.538	0.292	0.431	0.014	0.031
2009	0.874	0.951	0.126	0.049	0.000	0.000
2010	0.916	0.870	0.083	0.128	0.001	0.003
2011	0.908	0.898	0.092	0.102	0.000	0.000
2012	0.590	0.810	0.398	0.185	0.012	0.005
2013	0.859	0.871	0.139	0.128	0.002	0.001
2014	0.938	NA	0.062	NA	0.000	NA

TABLE 5. Fraction of burned Ha in La Primavera by level of severity. Here NA stands for *not available*.

Figure 10-B depicts the 2008 burned area which is, whimsically, located at Northeast and Southeast of La Primavera. The largest affected surface shows a low severity and a considerably smaller area exhibits moderate to high severity. Oak-pine forest and induced grasslands comprise the vegetation of this area. As mentioned above this event was known by

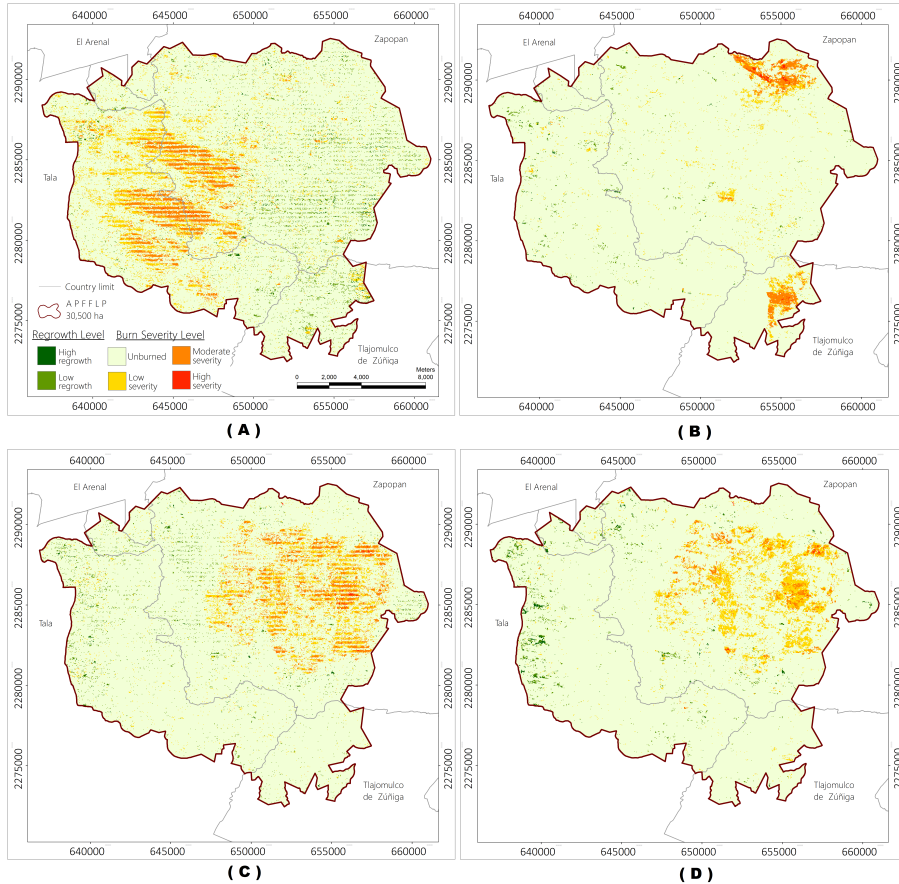


FIGURE 10. Burn severity maps. (A) 2005, $h = 0.15$. (B) 2008, $h = 0.23$. (C) 2012, $h = 0.15$. (D) 2012, $h = 0.23$.

the local authorities and they have reported that this fire might have been set intentionally. To this date there is not an official record on the total damaged area, see Huerta-Martínez and Ibarra-Montoya (2014) for more details. We consider that this map is an important piece of evidence that our approach can be used as an effective tool for monitoring burned areas, despite a high density of missing values, when satellite imagery time series are utilized.

Figure 10-C and D report on the 2012 burned area when using $h = 0.15$ and $h = 0.23$, respectively. The vast majority of this area has been categorized by low severity. In comparison, those areas with moderate and high severity are larger when using $h = 0.15$ than when using $h = 0.23$. Oak-pine forest and shrubby vegetation dominate this area. According to reports from the state of Jalisco, from 10 to 20% of wooded died as a result of fire which might have been started in a clandestine landfill.

In Section 5.3 we explore some strategies to enhance the appearance of our burn severity maps. Next, we validate our 2012 burn severity map and show that the overall accuracy of our product improves with the quality of the data set.

5.2. Accuracy assessment for a burn severity map.

In this section we follow Ch. 4 of Congalton and Green (2009) to assess the overall accuracy of our 2012 burn severity map. As reference data we use the RapidEye polygon of the 2012 burned area provided by CONABIO, see Section 2.2.1 for further details.

Spatial smoothing	h	Overall accuracy (%)		
		Whole area	Poor data quality	Moderate data quality
None	0.15	57.14	61.88	80.25
None	0.23	55.05	57.69	69.23
ArcMap filter	0.23	58.84	66.05	83.78
gdal_fillnodata	0.15	53.29	57.14	65.79

TABLE 6. Overall accuracy of 2012 burn severity map as a function of data quality. Spatial smoothing strategies are introduced in Section 5.3.

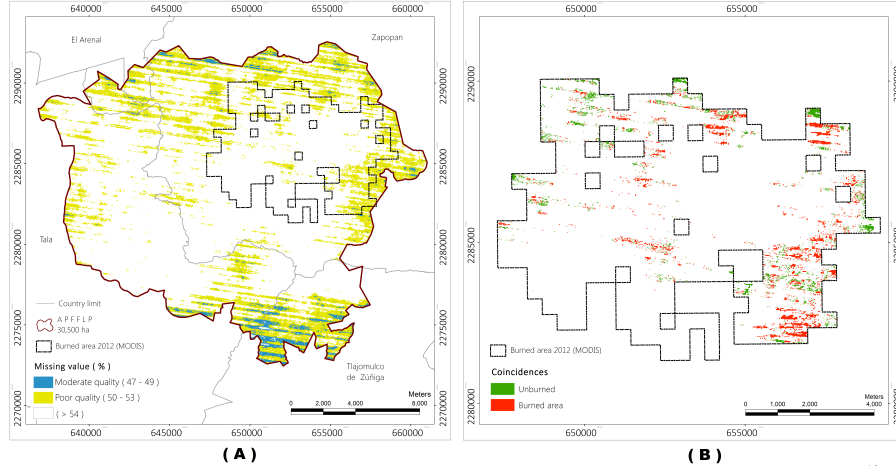


FIGURE 11. Overview of quality of data cube. (A) Percentage of missing values in each pixel. (B) Comparison between reference data (RapidEye polygon) and our 2012 burn severity map when only *Poor Quality* pixels are considered.

Technically speaking, in order to compute the overall accuracy, the burned and unburned area polygons provided by the RapidEye product were overlapped with those produced by our approach, yielding omission and commission errors which all were recorded in an error matrix; we employed some functions of ArcMap 10.3.1 to get these errors.

The overall accuracy is rather low, from 53 to 58%, when we employ all the pixels of the reference RapidEye polygon, see column Whole area in Table 6. We know from our simulations that data quality does have an effect in the performance of BFAST in detecting breakpoints which, in turn, arguably influences the accuracy of our product. Because of this we define a *mask* indicating the data quality of each pixel on the RapidEye polygon, see Figure 11-A. We associated the pixel quality with the percentage of missing data in its corresponding NDVI time series. For example, a *poor quality* pixel is that whose percentage of missing data ranges from 50 to 53% and a pixel with *moderate quality* is that exhibiting 47 to 49% of missing data. Having defined these classes we compute the corresponding overall accuracy. Figure 11-B shows the coincidences between the reference RapidEye polygon and our product when we only considered poor quality pixels; the columns Poor data quality and Moderate data quality in Table 6 are based on this mask.

In average, focusing only on the burned areas with poor quality pixels the overall accuracy improves 5%. This improvement, in average, reaches 19% when we consider areas with moderate quality pixels. This makes us confident that our methodology will work appropriately

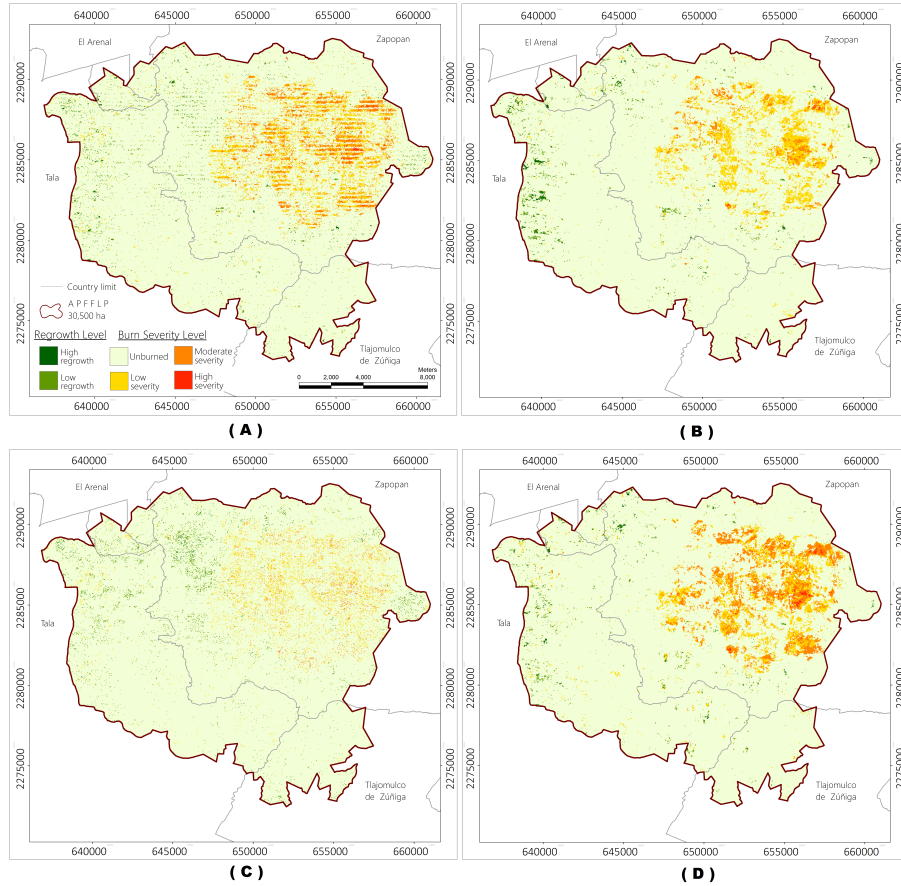


FIGURE 12. Burn severity maps for 2012. (A) $h = 0.15$. (B) $h = 0.23$. (C) $h = 0.23$ with ArcMap spatial smoothing. (D) $h = 0.15$ with `gdal_fillnodata` interpolation.

in determining the severity of burn areas provided the quality of the NDVI data cube is optimal.

5.3. Some strategies to enhance burned area detection.

Based on Figure 11-A, more than half of the pixels in the area of study lacks of at least 54% of observations. We have argued that our methodology is expected to produce reliable results as soon as the quality of the data sets improve. We have also argued that h , the bandwidth parameter required by the OLS-MOSUM test statistic, influences the total amount of breakpoints estimated each year. Consequently, it is plausible that the bandwidth also has an impact on the burned areas estimated by our approach. Now we discuss a few strategies that we implemented in order to try and enhance not only the appearance of our maps but also its overall accuracy.

As a working example we consider the burn severity maps for 2012. The discussion that follows is based on the maps shown in Figure 12 which, in turn, gave rise to the overall accuracy Table 6.

The first visual difference occurs when we utilize $h = 0.15$ or $h = 0.23$ as BFAST's bandwidth parameter, see **A** and **B**, respectively. In the former figure, the estimated burned area shows an apparent *banding* whereas the latter exhibits the burned area more *continuously*. Regardless of this continuous aspect, **A** seems to have estimated a larger burned area than

B. This feature is reflected in the overall accuracy of each of these maps, first two rows of Table 6, as the accuracy of map-**A** is larger than that of map-**B** across different data quality classes.

Next, we move to describe Figure 12-**C** and **D**. In both cases we first applied a spatial smoothing on the 238 Landsat-7 scenes and then we interpolated linearly the rest of the data cubes. For map-**C** we applied the ArcMap 10.3.1 low-pass filter with a 3×3 spatial kernel and for map-**D** we utilized the algorithm `gdal_fillnodata` from the GDAL library, cf. GDAL (2019). This algorithm uses the nodata flag `MaskBand`, a product that is available along with the Landsat-7 images, and interpolates the missing values from pixels in their vicinity; the process is finished by an iterative moving average filter with a 3×3 bandwidth. Visually, map-**D** is superior to map-**C** as it shows a realistic level of continuity in the burned area. Despite its *pixelated* look, the overall accuracy of map-**C** is larger than that of map-**D** and larger to any product in comparison for that matter.

We consider that the results of this section are encouraging to open a line of research about statistically-based *imputation* techniques for the Landsat-7 imagery and assess its impact, hopefully minimal, over the breakpoint estimation process. Having a complete, or well-imputed, data cube may cause that the role of the bandwidth parameter h be rather secondary. These ideas require further investigation and are outside the scope of the present article.

6. CONCLUSIONS

In its initial stage the methodology proposed in this paper allows for the semi-automatic (only one tuning parameter is needed) statistical estimation of abrupt changes (breakpoints) in the NDVI's trend structure; this idea has been applied for determining different disturbances (for instance, pests) in some ecosystems. In a second stage, our method permits for the identification of disturbances in forest attributed to fire. More precisely, by combining the statistical estimation of breakpoints in the NDVI's trend with the computation of the dNBR in a temporal vicinity of the estimated breakpoint our method allows for mapping burned area simply and appropriately. Unlike other methods, ours does not require prior knowledge of the burn's date.

All the above is possible due to the combination of the statistical estimation of breakpoints in the NDVI's trend with the computation of the dNBR in a temporal vicinity of the estimated breakpoint.

The simulation studies of this work serve 2 purposes. First, we calibrate some parameters needed in the statistical method to identify breakpoints in NDVI time series with a large amount of missing values. Then, our simulations contribute to a better comprehension of the role of the bandwidth parameter used by the OLS-MOSUM test to identify breakpoints. For instance, the latter allows us to determine that we need a rather small bandwidth, $h = 0.15$, in order to identify breakpoints in the first, and last, 2 years of our NDVI, Landsat-derived, 14 years long, time series. Also, we found that for the same type of time series, $h = 0.23$ prevents overestimation of the breakpoints. We envision that our discussion on the value of h , arguably the only tuning parameter of BFAST, alerts on the need for the development of a parameter-free statistical breakpoint estimation procedure with multiple applications for the remote sensing community. As a by-product, our simulations show that when in need

σ	methods	amplitude=0.15			amplitude=0.3		
		% of missing values					
		40	50	60	40	50	60
0.02	Linear	58.8	30.3	10.4	53.4	24.1	6.4
	Spline	72.6	54.0	42.8	80.8	65.9	53.0
0.05	Linear	58.1	37.3	13.0	57.6	29.1	8.6
	Spline	60.3	41.8	25.1	67.0	51.2	34.6
0.07	Linear	58.6	33.3	13.9	57.6	28.8	9.6
	Spline	56.9	38.9	20.6	59.1	41.3	27.5

TABLE 7. Probability coverage of estimating one breakpoint as a function of σ . Here bandwidth is $h = 0.15$.

of a simple method to fill in missing values which has a moderate impact on breakpoint estimation, we can rely on linear interpolation.

We showed empirically that our burn severity maps improve their overall accuracy as the quality of the data cubes improves. This makes us confident that the application of our methodology on optimal data cubes will contribute to an effective assessment of the severity of burned areas. We identify statistical imputation of Landsat-7 images and its influence on breakpoint estimation as a niche for future work.

It would also be interesting to apply our methodology in other areas to show its validity and usefulness in broader scenarios. It is also of great interest to extend the study period, perhaps with other products (Landsat-8, SENTINEL), and even consider other indexes such as the Enhanced Vegetation Index (EVI) as an auxiliary variable for mapping burned areas.

7. ACKNOWLEDGMENTS

This work was partly supported by Project No. 2760 from "Convocatoria de Proyectos de Desarrollo Científico para Atender Problemas Nacionales 2016", National Council of Science and Technology (CONACyT). The authors would like to thank to Lilia de Lourdes Manzo Delgado, Leticia Gómez Mendoza and Stéphane Couturier with the Institute of Geography at UNAM as well as to Rainer Ressler with CONABIO for helpful discussions and suggestions. Special thanks to Roberto Martínez with CONABIO for pointing out to the function `gdal_fillnodata`.

8. SUPPLEMENTARY MATERIALS

In this section we include maps, figures and tables which have been mentioned in the main document. When necessary we will add comments associated with the material presented here.

Discussion of Table 7. For the smallest variability level ($\sigma = 0.02$) and percentage of missing data (40%) both interpolation methods have their best performance. Overall, the greatest BFAST's probability coverage is achieved when the synthetic time series are interpolated with spline across all considered cases, especially for a marked amplitude (0.3). Also, the performance of any of the interpolation methods decays as the percentage of missing values increases.

Discussion of Figure 13. We consider underestimation, i.e. either τ_1 or τ_2 are estimated correctly, when one (top row), two (middle row) or more than two (bottom row) breakpoints are detected. In the first case, and regardless of the interpolation method, when 40% of data

h	methods	% of missing values						
		0	10	20	30	40	50	60
0.15	Linear	99.8	98.9	95.1	79.7	55.4	23.6	7.9
	Spline	99.8	99.1	95.6	88.7	79.4	67.5	53.3
0.23	Linear	100	99.9	98.4	92.4	78.1	56.1	35.1
	Spline	100	99.8	99.0	96.0	91.9	85.4	74.9
0.45	Linear	100	100	100	100	100	100	100
	Spline	100	100	100	100	100	100	99.9

TABLE 8. Probability coverage of estimating one breakpoint as a function of h and amplitude 0.3.

h	methods	% of missing values						
		0	10	20	30	40	50	60
0.15	Linear	100	99.4	95.7	80.6	54.9	22.6	6.9
	Spline	100	99.5	97.6	94.3	87.6	75.9	59.8
0.23	Linear	100	99.9	98.6	92.6	76.7	53.4	31.8
	Spline	100	99.9	99.4	98.3	95.4	89.4	78.8
0.45	Linear	100	100	100	100	100	100	100
	Spline	100	100	100	100	100	100	99.5

TABLE 9. Probability coverage of estimating one breakpoint as a function of h and amplitude 0.45.

h	methods	% of missing values						
		0	10	20	30	40	50	60
0.15	Linear	100	91.3	80.8	69.4	59.0	55.1	43.0
	Spline	100	91.3	80.4	69.2	61.5	49.0	35.3
0.23	Linear	100	91.4	80.7	70.6	61.7	53.8	45.3
	Spline	100	91.3	79.9	69.5	62.0	50.8	35.0
0.45	Linear	100	91.4	80.5	70.9	62.3	54.8	44.8
	Spline	100	91.3	80.0	70.0	61.7	50.8	35.2

TABLE 10. Correct estimation probability coverage for one breakpoint when h varies and amplitude 0.3.

h	methods	% of missing values						
		0	10	20	30	40	50	60
0.15	Linear	100	91.3	81.1	69.9	58.7	51.8	50.7
	Spline	100	91.1	79.7	68.9	59.7	46.5	28.6
0.23	Linear	100	91.4	81.0	71.1	62.1	56.6	44.7
	Spline	100	91.0	79.2	69.0	59.7	47.2	30.1
0.45	Linear	100	91.4	80.9	71.6	64.0	56.7	45.1
	Spline	100	91.0	79.3	69.5	59.8	47.0	31.0

TABLE 11. Correct estimation probability coverage for one breakpoint when h varies and amplitude 0.45.

are missing BFAST only underestimates when the separation between τ_1 and τ_2 is lesser than 40 time-points. In the second case (when two breakpoints are detected), independently of the percentage of missing data and the interpolation method, BFAST's underestimation reaches a stable level (45%) once the separation is about 50 time-points. Finally, when BFAST has detected more than two breakpoints independently of the missing data and the interpolation method, BFAST's underestimation reaches a stable level (50%). BFAST's underestimation

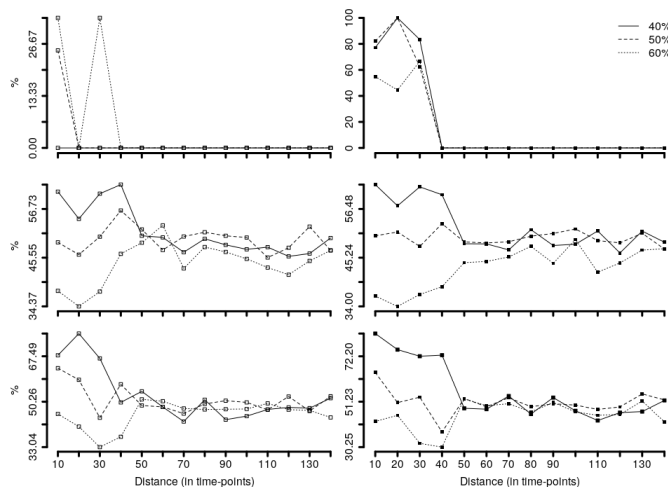


FIGURE 13. Underestimation. Bandwidth $h = 0.15$. Interpolation methods: left column (linear), right column (spline).

will not cease in this case. This is contrary to what we found for the case $h = 0.23$ when the underestimation ceases once the breakpoints are separated by at least 80 time-points.

REFERENCES

- Boschetti, L., Roy, D. P., Justice, C. O., and Humber, M. L. (2015). MODIS–Landsat fusion for large area 30 m burned area mapping. *Remote Sensing of Environment*, 161:27–42.
- Brewer, C. K., Winne, J. C., Redmond, R. L., Opitz, D. W., and Mangrich, M. V. (2005). Classifying and mapping wildfire severity. *Photogrammetric Engineering & Remote Sensing*, 71(11):1311–1320.
- Caetano, M., Mertes, L., Cadete, L., and Pereira, J. (1996). Assessment of AVHRR data for characterizing burned areas and post-fire vegetation recovery. *EARSeL Advances in Remote Sensing*, 4:124–134.
- Campagnolo, M., Oom, D., Padilla, M., and Pereira, J. (2019). A patch-based algorithm for global and daily burned area mapping. *Remote Sensing of Environment*, 232:111288.
- Chu, C.-S. J., Hornik, K., and Kaun, C.-M. (1995). MOSUM tests for parameter constancy. *Biometrika*, 82(3):603–617.
- Chuvieco, E. (2009). *Earth observation of wildland fires in Mediterranean ecosystems*. Springer.
- Chuvieco, E. and Congalton, R. G. (1988). Mapping and inventory of forest fires from digital processing of TM data. *Geocarto International*, 3(4):41–53.
- Chuvieco, E., Giglio, L., and Justice, C. (2008). Global characterization of fire activity: toward defining fire regimes from Earth observation data. *Global Change Biology*, 14(7):1488–1502.
- Chuvieco, E., Mouillot, F., van der Werf, G. R., San Miguel, J., Tanasse, M., Koutsias, N., García, M., Yebra, M., Padilla, M., Gitas, I., et al. (2019). Historical background and current developments for mapping burned area from satellite earth observation. *Remote sensing of environment*, 225:45–64.

- Chuvieco, E., Riaño, D., Danson, F., and Martin, P. (2006). Use of a radiative transfer model to simulate the postfire spectral response to burn severity. *Journal of Geophysical Research: Biogeosciences*, 111(G4).
- Cocke, A. E., Fulé, P. Z., and Crouse, J. E. (2005). Comparison of burn severity assessments using Differenced Normalized Burn Ratio and ground data. *International Journal of Wildland Fire*, 14(2):189–198.
- Congalton, R. G. and Green, K. (2009). *Assessing the accuracy of remotely sensed data: principles and practices*. CRC press, 2 edition.
- del Castillo, A. (2006). *La Primavera en llamas*. CONAFOR, 1 edition.
- Delgado-Morales, A. (2012). Combate de incendios forestales. *Sentidos de La Primavera*, 3:6–7.
- DeVries, B., Verbesselt, J., Kooistra, L., and Herold, M. (2015). Robust monitoring of small-scale forest disturbances in a tropical montane forest using Landsat time series. *Remote Sensing of Environment*, 161:107–121.
- Díaz-Delgado, R. (2003). Efecto de la recurrencia de los incendios sobre la resiliencia post-incendio de las comunidades vegetales de Cataluña a partir de imágenes de satélite. *Revista Ecosistemas*, 12(3).
- Doerr, S., Shakesby, R., Blake, W., Chafer, C., Humphreys, G., and Wallbrink, P. (2006). Effects of differing wildfire severities on soil wettability and implications for hydrological response. *Journal of Hydrology*, 319(1-4):295–311.
- Dutrieux, L. P., Verbesselt, J., Kooistra, L., and Herold, M. (2015). Monitoring forest cover loss using multiple data streams, a case study of a tropical dry forest in Bolivia. *ISPRS Journal of Photogrammetry and Remote Sensing*, 107:112–125.
- Eidenshink, J., Schwind, B., Brewer, K., Zhu, Z.-L., Quayle, B., and Howard, S. (2007). A project for monitoring trends in burn severity. *Fire ecology*, 3(1):3–21.
- Epting, J. and Verbyla, D. (2005). Landscape-level interactions of prefire vegetation, burn severity, and postfire vegetation over a 16-year period in interior alaska. *Canadian Journal of Forest Research*, 35(6):1367–1377.
- Escuin, S., Navarro, R., and Fernandez, P. (2008). Fire severity assessment by using NBR (Normalized Burn Ratio) and NDVI (Normalized Difference Vegetation Index) derived from Landsat TM/ETM images. *International Journal of Remote Sensing*, 29(4):1053–1073.
- Foga, S., Scaramuzza, P. L., Guo, S., Zhu, Z., Dille Jr, R. D., Beckmann, T., Schmidt, G. L., Dwyer, J. L., Hughes, M. J., and Laue, B. (2017). Cloud detection algorithm comparison and validation for operational Landsat data products. *Remote Sensing of Environment*, 194:379–390.
- GCOS (2019). Global climate observation system. <https://gcos.wmo.int/en/essential-climate-variables/ecv-factsheets>. [Online; accessed 18-November-2019].
- GDAL (2019). *GDAL/OGR Geospatial Data Abstraction software Library*. Open Source Geospatial Foundation.
- Giglio, L., Loboda, T., Roy, D. P., Quayle, B., and Justice, C. O. (2009). An active-fire based burned area mapping algorithm for the MODIS sensor. *Remote Sensing of Environment*, 113(2):408–420.
- Goodwin, N. R. and Collett, L. J. (2014). Development of an automated method for mapping fire history captured in landsat tm and etm+ time series across Queensland, Australia.

- Remote Sensing of Environment*, 148:206–221.
- Hawbaker, T. J., Vanderhoof, M. K., Beal, Y.-J., Takacs, J. D., Schmidt, G. L., Falgout, J. T., Williams, B., Fairaux, N. M., Caldwell, M. K., Picotte, J. J., et al. (2017). Mapping burned areas using dense time-series of landsat data. *Remote Sensing of Environment*, 198:504–522.
- Hermosilla, T., Wulder, M. A., White, J. C., Coops, N. C., and Hobart, G. W. (2015). An integrated Landsat time series protocol for change detection and generation of annual gap-free surface reflectance composites. *Remote Sensing of Environment*, 158:220–234.
- Huerta-Martínez, F. M. and Ibarra-Montoya, J. L. (2014). Incendios en el bosque La Primavera (Jalisco, México): un acercamiento a sus posibles causas y consecuencias. *CienciaUAT*, 9(1):23–32.
- INEGI (2016). Conjunto de datos vectoriales de uso del suelo y vegetación, escala 1:250 000, serie VI, México.
- Key, C. H. (2006). Ecological and sampling constraints on defining landscape fire severity. *Fire Ecology*, 2(2):34–59.
- Key, C. H. and Benson, N. C. (2006). Landscape Assessment (LA) Sampling and Analysis Methods. USDA Forest Service Gen. Technical report, Tech. Rep. RMRS-GTR-164-CD.
- Landsat Missions, U. (2016). United States Geological Survey USGS, section: About Landsat.
- Lutes, D. C., Keane, R. E., Caratti, J. F., Key, C. H., Benson, N. C., Sutherland, S., and Gangi, L. J. (2006). Firemon: Fire effects monitoring and inventory system. *Gen. Tech. Rep. RMRS-GTR-164. Fort Collins, CO: US Department of Agriculture, Forest Service, Rocky Mountain Research Station. 1 CD.*, 164.
- Martín, M. and Chuvieco, E. (2001). Propuesta de un nuevo índice para cartografía de áreas quemadas: aplicación a imágenes NOAA-AVHRR y Landsat-TM. *Revista de Teledetección*, 16:57–64.
- Masek, J. G., Vermote, E. F., Saleous, N. E., Wolfe, R., Hall, F. G., Huemmrich, K. F., Gao, F., Kutler, J., and Lim, T.-K. (2006). A Landsat surface reflectance dataset for North America, 1990-2000. *IEEE Geoscience and Remote Sensing Letters*, 3(1):68–72.
- Miller, J. D. and Thode, A. E. (2007). Quantifying burn severity in a heterogeneous landscape with a relative version of the delta Normalized Burn Ratio (dNBR). *Remote Sensing of Environment*, 109(1):66–80.
- Miller, J. D. and Yool, S. R. (2002). Mapping forest post-fire canopy consumption in several overstory types using multi-temporal Landsat TM and ETM data. *Remote Sensing of Environment*, 82(2-3):481–496.
- Moody, J. A., Shakesby, R. A., Robichaud, P. R., Cannon, S. H., and Martin, D. A. (2013). Current research issues related to post-wildfire runoff and erosion processes. *Earth-Science Reviews*, 122:10–37.
- Moritz, S. and Bartz-Beielstein, T. (2017). imputeTS: time series missing value imputation in R. *The R Journal*, 9(1):207–218.
- Pyne, S. J. (1997). *World fire: the culture of fire on earth*. University of Washington Press.
- Robichaud, P. R., Lewis, S. A., Laes, D. Y., Hudak, A. T., Kokaly, R. F., and Zamudio, J. A. (2007). Postfire soil burn severity mapping with hyperspectral image unmixing. *Remote Sensing of Environment*, 108(4):467–480.

- Rogan, J. and Yool, S. (2001). Mapping fire-induced vegetation depletion in the Peloncillo Mountains, Arizona and New Mexico. *International Journal of Remote Sensing*, 22(16):3101–3121.
- Roy, D. P., Boschetti, L., and Trigg, S. N. (2006). Remote sensing of fire severity: assessing the performance of the normalized burn ratio. *IEEE Geoscience and Remote Sensing Letters*, 3(1):112–116.
- Roy, D. P., Huang, H., Boschetti, L., Giglio, L., Yan, L., Zhang, H. H., and Li, Z. (2019). Landsat-8 and Sentinel-2 burned area mapping- A combined sensor multi-temporal change detection approach. *Remote Sensing of Environment*, 231:111254.
- Schultz, M., Clevers, J. G., Carter, S., Verbesselt, J., Avitabile, V., Quang, H. V., and Herold, M. (2016). Performance of vegetation indices from Landsat time series in deforestation monitoring. *International Journal of Applied Earth Observation and Geoinformation*, 52:318–327.
- Semarnat (2000). Programa de manejo Área de Protección de Flora y Fauna La Primavera.
- Stroppiana, D., Bordogna, G., Boschetti, M., Carrara, P., Boschetti, L., and Brivio, P. A. (2011). Positive and negative information for assessing and revising scores of burn evidence. *IEEE Geoscience and Remote Sensing Letters*, 9(3):363–367.
- UN (2019). Sustainable development goals. <https://sustainabledevelopment.un.org/sdg15>. [Online; accessed 18-November-2019].
- Van Wagtendonk, J. W. and Root, R. R. (2003). The use of multi-temporal Landsat Normalized Difference Vegetation Index (NDVI) data for mapping fuel models in Yosemite National Park, USA. *International Journal of Remote Sensing*, 24(8):1639–1651.
- Van Wagtendonk, J. W., Root, R. R., and Key, C. H. (2004). Comparison of AVIRIS and Landsat ETM+ detection capabilities for burn severity. *Remote Sensing of Environment*, 92(3):397–408.
- Verbesselt, J., Hyndman, R., Newnham, G., and Culvenor, D. (2010a). Detecting trend and seasonal changes in satellite image time series. *Remote Sensing of Environment*, 114(1):106–115.
- Verbesselt, J., Hyndman, R., Zeileis, A., and Culvenor, D. (2010b). Phenological change detection while accounting for abrupt and gradual trends in satellite image time series. *Remote Sensing of Environment*, 114(12):2970–2980.
- Verbesselt, J., Zeileis, A., Hyndman, R., and Verbesselt, M. J. (2012). Package bfast.
- Vermote, E. F., Tanré, D., Deuze, J. L., Herman, M., and Morcette, J.-J. (1997). Second simulation of the satellite signal in the solar spectrum, 6s: An overview. *IEEE Transactions on Geoscience and Remote Sensing*, 35(3):675–686.
- Watts, L. M. and Laffan, S. W. (2014). Effectiveness of the BFAST algorithm for detecting vegetation response patterns in a semi-arid region. *Remote Sensing of Environment*, 154:234–245.
- Whelan, R. J. (1995). *The ecology of fire*. Cambridge University Press.
- White, J., Wulder, M., Hobart, G., Luther, J., Hermosilla, T., Griffiths, P., Coops, N., Hall, R., Hostert, P., Dyk, A., et al. (2014). Pixel-based image compositing for large-area dense time series applications and science. *Canadian Journal of Remote Sensing*, 40(3):192–212.
- Wu, Q., Liu, K., Song, C., Wang, J., Ke, L., Ma, R., Zhang, W., Pan, H., and Deng, X. (2018). Remote sensing detection of vegetation and landform damages by coal mining on the Tibetan Plateau. *Sustainability*, 10(11):3851.

- Zeileis, A., Leisch, F., Hornik, K., and Kleiber, C. (2002). strucchange: An R package for testing for structural change in linear regression models. *Journal of Statistical Software, Articles*, 7(2):1–38.
- Zewdie, W., Csaplovics, E., and Inostroza, L. (2017). Monitoring ecosystem dynamics in northwestern Ethiopia using NDVI and climate variables to assess long term trends in dryland vegetation variability. *Applied geography*, 79:167–178.
- Zhang, C., Li, W., and Travis, D. (2007). Gaps-fill of SLC-off Landsat ETM+ satellite image using a geostatistical approach. *International Journal of Remote Sensing*, 28(22):5103–5122.
- Zhao, F., Huang, C., and Zhu, Z. (2015). Use of vegetation change tracker and support vector machine to map disturbance types in greater yellowstone ecosystems in a 1984–2010 landsat time series. *IEEE Geoscience and Remote Sensing Letters*, 12(8):1650–1654.